Deep Scatter Estimation for Coarse Anti-Scatter Grids as used in Photon-Counting CT

Julien Erath[1, 2, 3], Jan Magonov[1, 2, 3], Joscha Maier[2], Eric Fournié[1], Martin Petersilka[1], Karl Stierstorfer[1], and Marc Kachelrieß[3]

[1]Siemens Healthineers (Forchheim, Germany)
[2]German Cancer Research Center (DKFZ) (Heidelberg, Germany)
[3]Heidelberg University (Heidelberg, Germany)

ABSTRACT

Due to the smaller detector pixels in photon-counting CT, coarse anti-scatter grids are used. This may lead to high frequencies in the scattered radiation and therefore moiré artifacts in the reconstructed images can occur. It has been shown that deep convolutional neural networks are very effective to correct scatter artifacts in clinical CT. In this work we present an adapted version of the deep scatter estimation (DSE) to correct for the high frequency artifacts effectively. With the use of DSE the mean absolute error of the scatter artifacts is reduced from about 8 HU to under 1 HU. At the same time the moiré artifacts can be prevented and additional post-processing in the image can be avoided.

1. INTRODUCTION

Recently the U.S. Food and Drug Administration (FDA) has cleared the world's first photon-counting computed tomography (CT) scanner, the Siemens NAEOTOM Alpha. The FDA described it as the first major new technology for computed tomography imaging in nearly a decade. Since its introduction, photon-counting detectors have shown a great potential to improve the spectral and spatial resolution of CT imaging.[1] The spectral information can be used for several different image techniques, for example virtual monochromatic imaging or iodine overlays. These possibilities can improve the clinical diagnostic of CT. To avoid the pulse pile-up effect and to improve the spatial resolution, the detector of the new photon-counting CT has very small detector pixels.[2–4] This can be useful to visualize, for example, small pulmonary vessels[5] or to show details of the inner ear.[6]

Scattered radiation and the resulting image artifacts are well-known in clinical CT. Generally, there are two strategies to minimize the effect of scatter, first to reduce the measured scattered radiation with special hardware like anti-scatter grids (ASG) and second to correct the scatter in the pre-processing of the image reconstruction. To achieve the best possible image quality these two techniques should be combined.

The use of the smaller detector pixels influences the effect of the scattered radiation in the detectors. For energy integrating detector each pixel is surrounded by the lamella of the ASG. Since with the photon-counting CT the detector pixels are much smaller, several pixels are combined between the lamellae of the ASG (left side in figure 1). This results in the fact that, dependent on the location and the angle of the incoming scattered photon, the scatter intensity can vary between the adjacent pixels in one ASG block. On the right side of figure 1 it can be seen that, depending on the angle of incidence, some photons will be absorbed by the anti-scatter grid and other will be measured in the detector. For energy-integrating detectors scattered intensities are usually low-frequency and only slowly change across the detector. These additional high frequencies in the scattered radiation can lead to ring artifacts in the reconstructed CT images, as shown in figure 2.

We have recently shown the efficient use of deep convolutional neural networks (CNN) to correct for scatter artifacts in clinical CT with the deep scatter estimation (DSE).[7–9] Once trained, the CNNs can lead to a very robust and fast scatter estimation. In this work, we propose the use of neural networks to correct for the artifacts resulting from coarse anti-scatter grids. Based on our previous work, we have modified the architecture of our neural network to estimate the new high frequencies in the occurring scattered radiation.

Corresponding author: Julien Erath (julien.erath@siemens-healthineers.com)

7th International Conference on Image Formation in X-Ray Computed Tomography,
edited by Joseph Webster Stayman, Proc. of SPIE Vol. 12304, 123040J
 · 0277-786X · doi: 10.1117/12.2646580

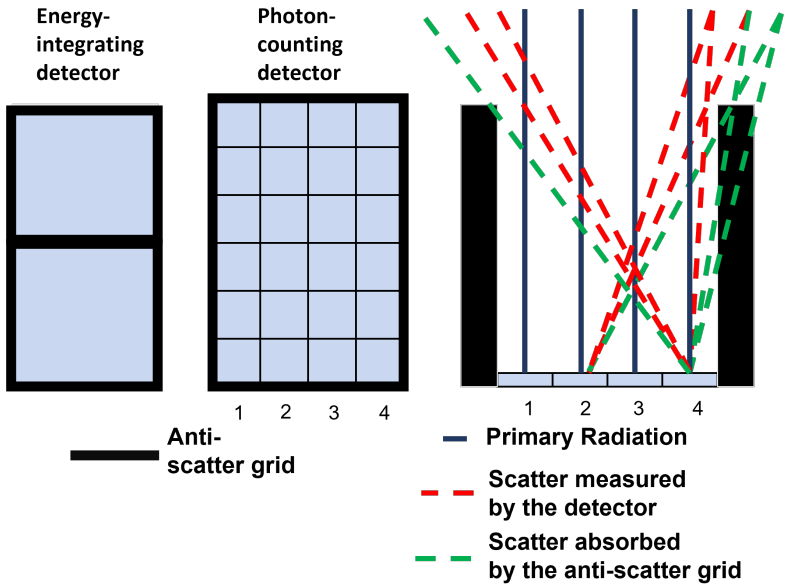

Figure 1. In energy-integrating detectors each pixel is surrounded by the lammela of the anti-scatter grid. In a photon-counting detector there are several pixels between the lamellae. Depending on the direction of the incoming scatter photon, it will be absorbed by the anti-scatter grid. Thus two neighboring pixels will receive a different scatter intensity.

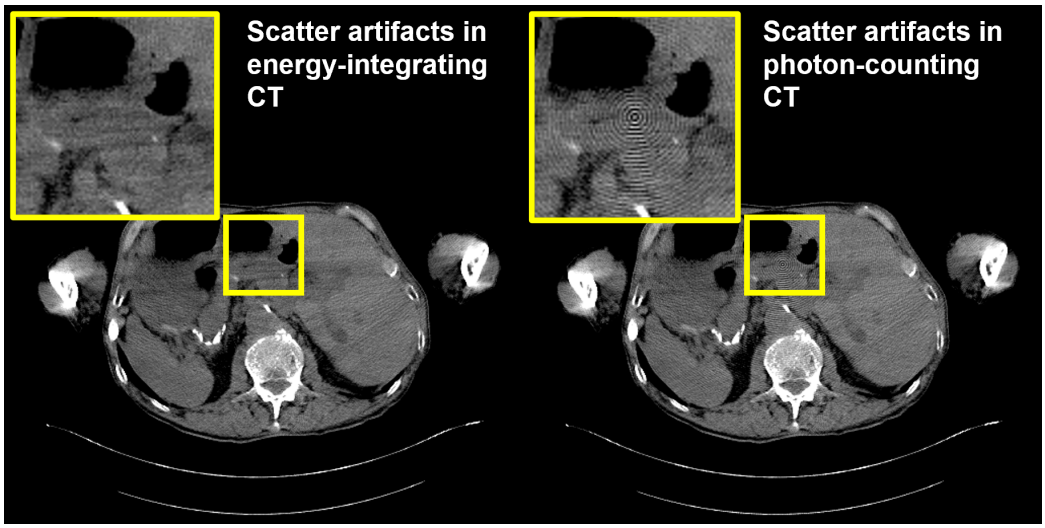

Figure 2. Illustration of the moiré effect due to the use of coarse anti-scatter grids in photon-counting CT.

2. METHODS AND MATERIAL

2.1 Data generation

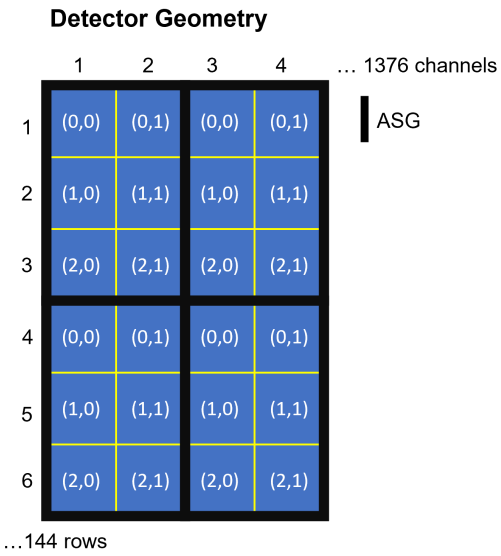

Figure 3. Simulated detector geometry. There are six different pixel locations within the anti-scatter grid which will measure a different intensity of scattered radiation. The total detector size is 1376×144 pixels, consisting of 688×48 of the six-pixel-blocks.

To obtain the scatter data for the neural network, we have adapted our in-house Monte-Carlo simulation[10] to the geometry of the photon-counting scanner NAEOTOM Alpha (Siemens Healthineers). In contrast to an energy-integrating detector where each pixel is surrounded by the lamella of the ASG, a coarse anti-scatter grid is used where 2×3 pixels are located between the lamellae of the ASG. The total detector size is 1376×144 pixels. As shown in figure 3, there are six different pixel locations under the coarse anti-scatter grid. If only one location is considered, the scattered radiation is further low-frequency. To consider this, post-smoothing needs to smooth only across same pixel locations and must not smooth between neighboring pixels. The distribution of the attenuation coefficient for the simulation of the CT scans is obtained from clinical full body CT exams. The patients are assumed to consist of four different materials (air, adipose tissue, soft tissue, and bone). One of these materials is assigned to each voxel based on CT value thresholds. In total 16 patients at 14 z-positions are Monte Carlo simulated in 10° steps. Twelve patients are used for training, two patients are used as validation data during the training and two patients are used as test data to evaluate the robustness of the networks. The corresponding primary intensities are obtained with a polychromatic forward projection. Overall 8064 paired scatter and primary data pairs are obtained for training and evaluation of the networks.

2.2 Deep scatter estimation

DSE is trained to predict scatter based on the acquired projection data as input.[7] In general DSE can be trained with measured or simulated scatter intensities.[11] Here the Monte Carlo-simulated scatter data will be used as the training and validation data. To adapt the network architecture to a coarse ASG the network receives the six different pixel locations as separate input channels (figure 4). The network is trained to predict six different output channels of the pixel locations, which then can be merged to obtain the scatter estimation for the whole detector. Each input and output channel has the size of 688×48 pixels.

2.3 Reconstruction

To evaluate the performance of the algorithm the scatter-corrected projections are reconstructed with the extended parallel back-projection (EPBP) algorithm.[12] Image quality is evaluated for the reconstructed images with the mean absolute error (MAE) compared to the ground truth. In the calculation of the MAE, air is excluded and only the patient area is considered.

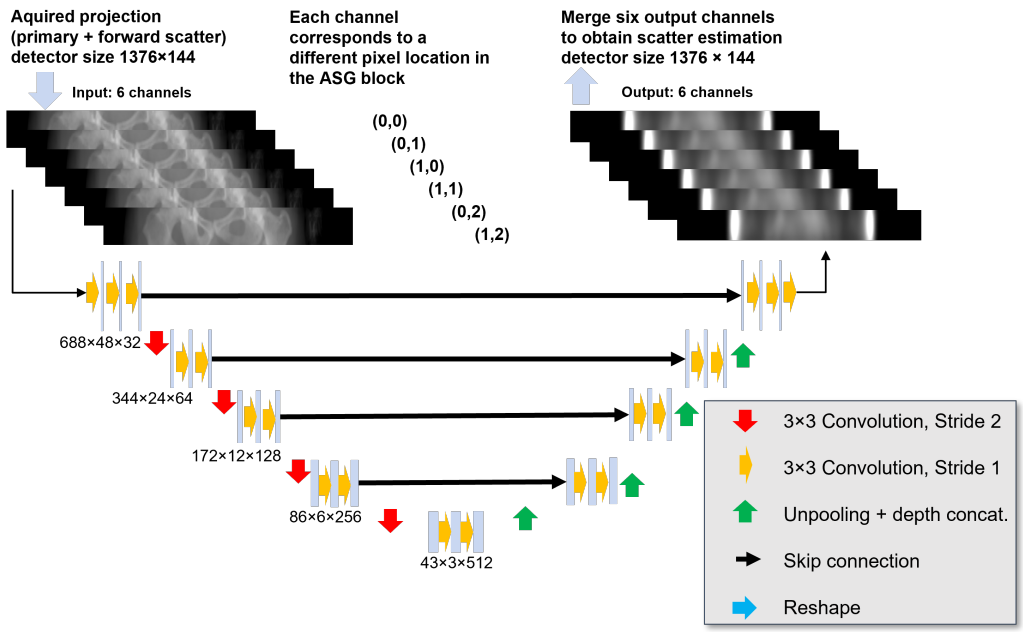

Figure 4. The neural network has six different input and output channels corresponding to the different pixel locations in the ASG.

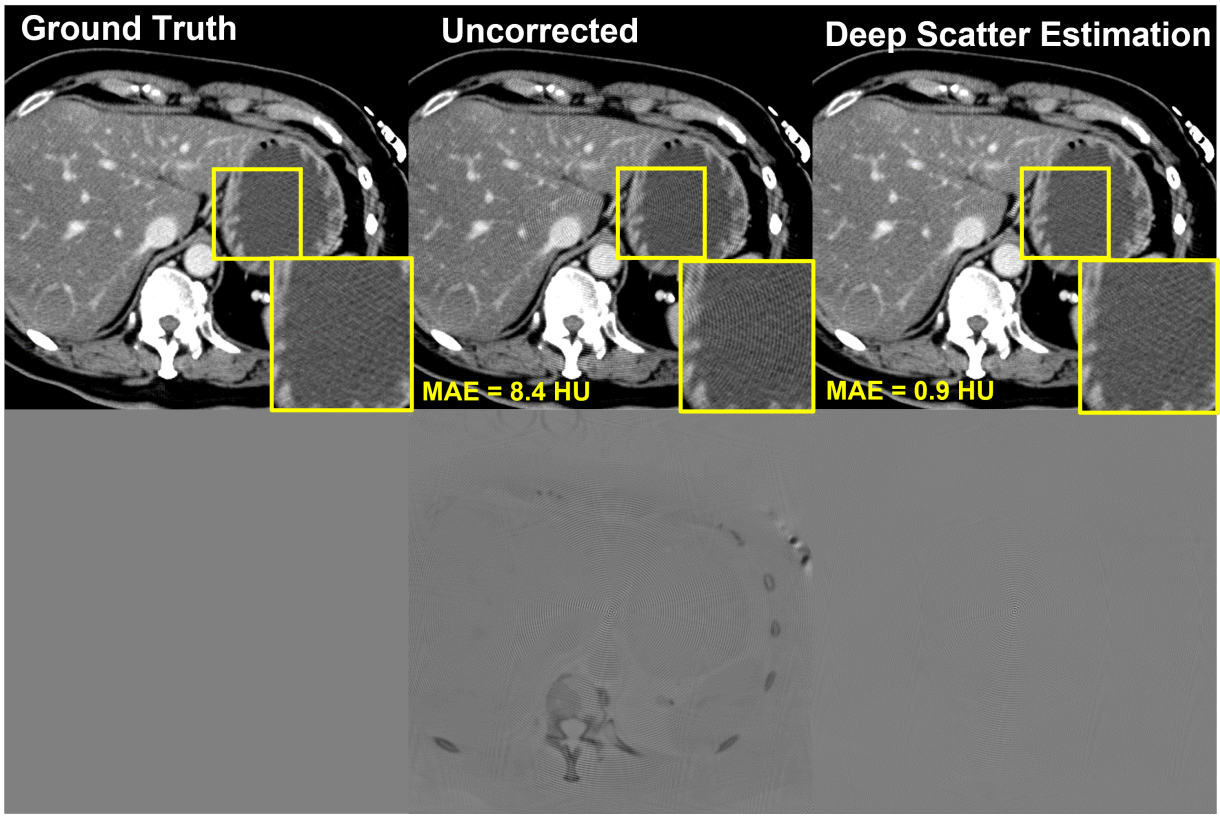

Figure 5. First example of DSE for coarse ASGs. With the proposed neural network the MAE gets reduced from 8.4 HU to 0.9 HU. In the enlarged area it can be seen that the moiré artifacts gets corrected. $C = 0$ HU, $W = 400$ HU. Difference to GT: $C = 0$ HU, $W = 50$ HU.

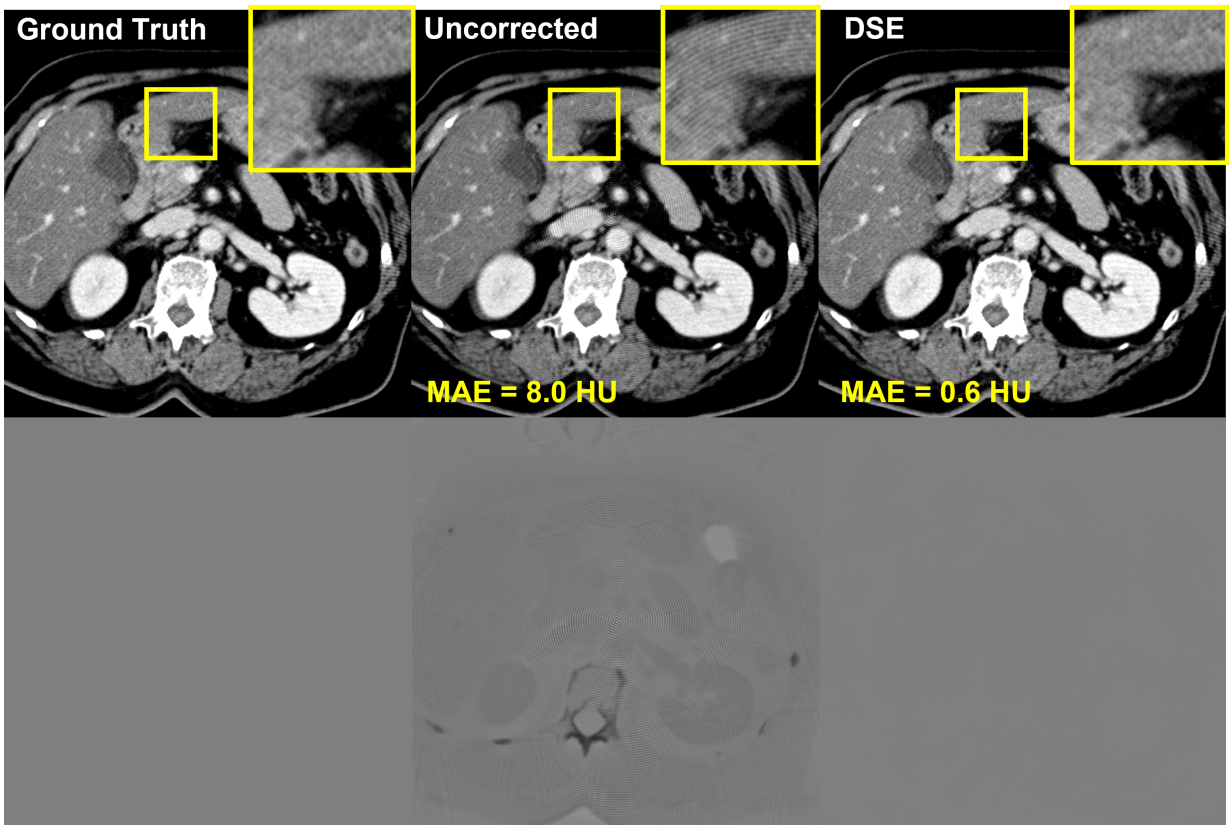

Figure 6. Second example of DSE for coarse ASGs. Here the algorithm reduces the MAE from 8.0 HU to 0.6 HU. In the difference image, it is visible that the networks corrects both the scatter and moiré artifacts. $C = 0$ HU, $W = 400$ HU. Difference to GT: $C = 0$ HU, $W = 50$ HU.

3. RESULTS

A clear moiré effect is visible in the reconstructed images without scatter correction. The average MAE in the uncorrected images is 8.4 HU. With the proposed algorithm the ring artifacts that appear can be significantly reduced and the average MAE is decreased to an average of 0.6 HU. In figures 5 and 6 two examples of the scatter correction are shown. In the enlarged area, it is visible that the moiré effect is corrected. The difference images also show that the DSE algorithm corrects the scatter artifacts very well.

4. DISCUSSION

We propose a deep learning-based method to correct for scatter artifacts in photon-counting CT. In this work we demonstrate the potential of DSE to correct the artifacts that may occur due to the smaller detector pixel size and the coarse anti-scatter grid. The neural network is able to leverage information about the different pixel locations and shows an accurate scatter estimation. The results presented are based on simulated data, but the algorithm can also be applied to clinical measurements. In our following step we plan to use the spectral information of the photon-counting detectors to further improve the scatter corrections.

ACKNOWLEDGMENTS

The Monte Carlo software RayConStruct-MC was provided by RayConStruct® GmbH, Nürnberg, Germany.

REFERENCES

[1] M. Lell and M. Kachelrieß, "Recent and upcoming technological developments in computed tomography: high speed, low dose, deep learning, multienergy," *Invest. Radiol.*, vol. 55, no. 1, pp. 8–19, 2020.

[2] K. Taguchi, E. C. Frey, X. Wang, J. S. Iwanczyk, and W. C. Barber, "An analytical model of the effects of pulse pileup on the energy spectrum recorded by energy resolved photon counting x–ray detectors," *Med. Phys.*, vol. 37, no. 8, pp. 3957–3969, Aug. 2010.

[3] K. Taguchi, M. Zhang, E. C. Frey, and X. Wang, "Modeling the performance of a photon counting x–ray detector for CT: Energy response and pulse pileup effects," *Med. Phys.*, vol. 38, no. 2, pp. 1089–1102, Feb. 2011.

[4] L. Klein, S. Dorn, C. Amato, S. Heinze, M. Uhrig, H.-P. Schlemmer, M. Kachelrieß, and S. Sawall, "Effects of detector sampling on noise reduction in clinical photon–counting whole–body computed tomography," *Investigative Radiology*, vol. 55, no. 2, pp. 111–119, Feb. 2020.

[5] S. Leng, K. Rajendran, H. Gong, W. Zhou, A. F. Halaweish, A. Henning, S. Kappler, M. Baer, J. G. Fletcher, and C. H. McCollough, "150-μm spatial resolution using photon-counting detector computed tomography technology: technical performance and first patient images," *Invest. Radiol.*, vol. 53, no. 11, pp. 655–662, 2018.

[6] A. Pourmorteza, R. Symons, A. Henning, S. Ulzheimer, and D. A. Bluemke, "Dose efficiency of quarter-millimeter photon-counting computed tomography: first-in-human results," *Invest. Radiol.*, vol. 53, no. 6, pp. 365–372, 2018.

[7] J. Maier, S. Sawall, M. Knaup, and M. Kachelrieß, "Deep scatter estimation (DSE): Accurate real-time scatter estimation for x-ray CT using a deep convolutional neural network," *Journal of Nondestructive Evaluation*, vol. 37, no. 3, p. 57, Jul. 2018.

[8] J. Maier, E. Eulig, T. Vöth, M. Knaup, J. Kuntz, S. Sawall, and M. Kachelrieß, "Real-time scatter estimation for medical CT using the deep scatter estimation: Method and robustness analysis with respect to different anatomies, dose levels, tube voltages, and data truncation," *Med. Phys.*, vol. 46, no. 1, pp. 238–249, Nov. 2019.

[9] J. Erath, T. Vöth, J. Maier, E. Fournié, M. Petersilka, K. Stierstorfer, and M. Kachelrieß, "Deep learning-based forward and cross-scatter correction in dual-source CT," *Medical Physics*, vol. 48, no. 9, pp. 4824–4842, 2021.

[10] M. Baer and M. Kachelrieß, "Hybrid scatter correction for CT imaging," *Phys. Med. Biol.*, vol. 57, pp. 6849–6867, 2012.

[11] J. Erath, J. Maier, E. Fournie, T. Vöth, K. Stierstorfer, and M. Kachelrieß, "Monte Carlo–free deep scatter estimation (DSE) for x-ray CT and CBCT." *Program of the 105th Scientific Assembly and Annual Meeting of the RSNA*, pp. SSE24–06, Dec. 2019.

[12] M. Kachelrieß, M. Knaup, and W. A. Kalender, "Extended parallel backprojection for standard 3D and phase–correlated 4D axial and spiral cone–beam CT with arbitrary pitch and 100% dose usage," *Med. Phys.*, vol. 31, no. 6, pp. 1623–1641, Jun. 2004.